Interactive simulation of plume and pyroclastic volcanic ejections

Maud Lastic
LIX, École Polytechnique, CNRS, IP Paris

Damien Rohmer
LIX, École Polytechnique, CNRS, IP Paris

Guillaume Cordonnier
Inria, Université Côte d'Azur

Claude Jaupart
Institut de Physique du Globe de Paris

Fabrice Neyret
LJK, CNRS, U-Grenoble, Inria

Marie-Paule Cani
LIX, École Polytechnique, CNRS, IP Paris

Figure 1: Interactive simulation (left) and off-line rendering of ejection phenomena during volcanic eruption: Rising column under the wind (middle); Pyroclastic flow (right), where secondary columns are generated along the way.

ABSTRACT

We propose an interactive animation method for the ejection of gas and ashes mixtures in volcano eruption. Our novel, layered solution combines a coarse-grain, physically-based simulation of the ejection dynamics with a consistent, procedural animation of multi-resolution details. We show that this layered model can be used to capture the two main types of ejection, namely ascending plume columns composed of rapidly rising gas carrying ash which progressively entrains more air, and pyroclastic flows which descend the slopes of the volcano depositing ash, ultimately leading to smaller plumes along their way. We validate the large-scale consistency of our model through comparison with geoscience data, and discuss both real-time visualization and off-line, realistic rendering.

CCS CONCEPTS

• **Computing methodologies** → **Procedural animation**; **Physical simulation**.

KEYWORDS

Computer animation, Natural phenomena, Procedural models

ACM Reference Format:
Maud Lastic, Damien Rohmer, Guillaume Cordonnier, Claude Jaupart, Fabrice Neyret, and Marie-Paule Cani. 2022. Interactive simulation of plume and pyroclastic volcanic ejections. In *Proceedings of Make sure to enter the correct conference title from your rights confirmation emai (I3D '22).* ACM, New York, NY, USA, Article 5770950, 9 pages. https://doi.org/10.1145/3522609

I3D '22, May 03–05, 2022

1 INTRODUCTION

As many myths and legends attest, volcanic eruptions are one of the natural phenomena that struck humans the most, due to their unique combination of stunning beauty and destructive power. As still popular storytelling element in movies and games, volcanic phenomena are nowadays monitored and analyzed for natural risks prevention, accurately modeled for better understanding and prediction, as well as explained to children at school or to the public in museums. Several of these applications, from education, museography, and communication about risks, to special effects (VFX) previsualization and games, share the need for an efficient, yet visually realistic, animated model for volcano eruption. In this paper, we tackle a part of this challenge, namely the interactive simulation of volcano's ejection columns and pyroclastic flows.

While volcano ejection was not much studied in Computer Graphics (CG) so far, smoke on one hand, and convective clouds on the other hand attracted a lot of work, leading to efficient simulation methods for combustion and condensation phenomena, respectively, using Eulerian methods in bounded domains. Existing software such as SideFX-Houdini [21] propose to reuse these as a default model for volcanic ejection. In addition to not allowing real-time interaction, these simulations however fail to capture the specific dynamics and visual appearance of real eruption recordings.

Indeed, to be plausible, simulations of volcanic ejection need to handle the two following specific features: First, the combination of extremely large size scales – as volcanic columns can expand for tens of kilometers vertically and hundreds horizontally – with fine details at the scale of a meter starting from ground level. Catching these two key scales is mandatory to allow close-ups and fly-overs. Second, the specific dynamic behavior of plume columns, as the eruptive material is initially expelled at high speed – close to the speed of sound – and with a density hundred times higher than the

density of the surrounding atmosphere. These extreme initial conditions lead to two unique emerging behaviors, drastically different from those of clouds or smoke: either a pyroclastic flow spreading down the slopes of the volcano, or an ascending plume propagating upward and finally spreading side-way at high altitude. To capture these specific large-scale behaviors, the reciprocal interaction between the highly turbulent, dense flow and the surrounding atmosphere must be accurately computed.

Efficiently capturing such inherent relationships between small and large scales, within an open environment, would be extremely difficult using traditional grid-based simulations. Therefore, we resort to the use of a layered animated model, which can be seen as the combination of simple and consistently coupled sub-models. More precisely, we combine minimalist Lagrangian simulation at medium scale, used to represent dynamic horizontal slices of material ejected by the volcano and interacting with the surrounding air, with a procedural model that enhances the visual animation of the turbulent flow with multi-resolution details.

Our technical contributions are threefold:

- We propose an efficient, yet consistent model for volcanic column dynamics at medium and large scales, based on a simple Lagrangian simulation inspired from prior knowledge and behavioral laws from volcanology studies.
- We introduce a procedural enrichment inspired by Kolmogorov cascades, to capture the complex motion of turbulent ashes and represent fine details up to a meter.
- We extend the previous two-layers model to capture pyroclastic flow propagation and the resulting sub-columns.

We validate the consistency of our solution through comparison with predictive models from volcanology literature, regarding the evolution of velocity and density over time and height, the shape profile of columns, and the maximal altitude of the plume. Lastly, we discuss two rendering techniques: a real-time pre-visualization method well suited to artistic modeling pipelines where manual tuning should be facilitated to enable fine-grain control; and off-line, volumetric rendering, enabling to compute realistic animations that can be visually compared with real images.

2 RELATED WORK

2.1 Simulating volcanoes in Computer Graphics

While lava flows attracted a lot of CG research [7, 10, 16, 22, 25, 36], the only work that tackled the simulation of volcanic columns was the early work from Mizuno et al. [14]. An Eulerian simulation on a coarse cubic grid of 100^3 voxels was used to compute the dynamics of ejected material. A procedural decrease, function of the height, was used for the density of the material. It did not take into account the velocity of the ejection, thus failing to capture the interaction between high-speed ejected material and the surrounding air. In addition, the use of a fixed cubic grid limited the representation of small-scale details while being computationally intensive. In contrast, our approach relies on ejection-air interaction laws. It is therefore able to automatically capture both buoyant ejection and pyroclastic flows. Moreover, it enables a real-time visual simulation of volcanic ejection, while spanning from small to large space scales.

Smoke simulations were extensively studied in CG, mostly using Eulerian grid-based methods [6, 11, 24]. Until recently, an impressive body of works, beyond the scope of this paper, have been dedicated to the improvement of these methods, in either accuracy, robustness, or efficiency (see [30] for a comprehensive survey). Indeed, smoke simulation at large spatial scales can be highly intensive in memory and computation usage. Performances were improved using moving grids able to follow the flow motion [20], or sub-grids able to merge and split [18]. Another solution was to run a coarse simulation and later enhance it with details [19], an approach recently improved using learning-based methods [33].

Closer to the high-speed, turbulent, and dense gas ejected by volcanoes, weather phenomena such as cloud formation share the challenge of combining large spatial extents with small-scale details. Similar to cloud simulation methods [8, 11, 31], we model thermal transfer and buoyancy. However, existing solutions cannot be reused in our case. Indeed, volcanic eruptions involve much higher velocities, drastic density and buoyancy variations, and high turbulence, which may either cause stability or integrity issues or would require too small time steps to achieve interactive simulation.

Lagrangian approaches are better suited to open domains than Eulerian grids but prove costly as well when many particles need to be used. Several methods relied on the enhancement of coarse-grain particle systems with procedural models, aimed at conveying details. A hierarchy of procedural spheres, rolling over each other, was introduced in the early work from Neyret [17] in the context of the animation of billowing clouds. This approach was also used in VFX: PDI and Digital Domain used rolling sphere representations to model dragon flames and avalanches [5, 12]. In this work, we rely on a similar, procedural approach to add details to our simulations.

In addition to their suitability for large, open domains, Lagrangian methods allow for the accurate modeling of vorticity in billowing phenomena: Vortex particles [3] enable to accurately locate vortices, concentrating the simulation cost to useful regions only. Angelidis [1] introduced vortex filaments instead of particles, to improve the conservation of vorticity energy, momentum, and strength. Despite performance improvements [32], such simulation would however get costly for large and detailed billowing objects such ad volcanic columns. Therefore, rather than tracking and simulating the distortions of vortex filaments, we directly model the dynamics of average "ring layers" throughout an eruptive column. The appearance of the billowing cascade is achieved by combining this Lagrangian simulation with procedural animated details.

2.2 Volcanic column models in geoscience

The formation of volcanic plumes was extensively studied in natural sciences. Volcanic columns are modeled as multiphasic flows, simulated using CFD codes on discretized domains [4, 13]. These models are extremely costly and require hours to days of computations. As volcanic plumes can rise over tens of kilometers before reaching their equilibrium altitude, coarse spatial resolutions are used, with voxels typically spanning a hundred meters. Therefore, only large-scale phenomena such as the plume expansion as well as macroscopic chemical and thermodynamic exchanges are captured [26, 29], while smaller scale phenomena are only averaged. Spatial resolution is too coarse to reproduce the visual appearance

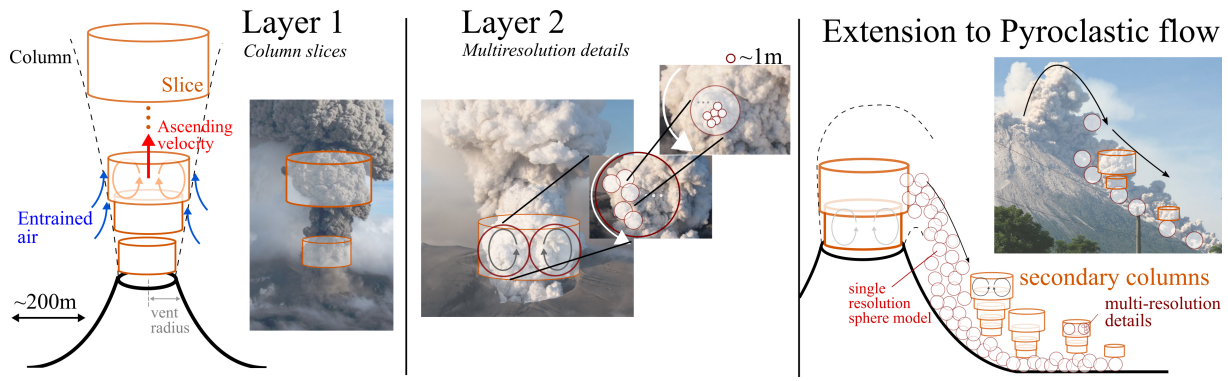

Figure 2: Our layered model makes use of circular slices to simulate and display the dynamics of the column (left), generates animated spheres at different resolutions to model small-scale visual details (middle), and provides an extension of these layers to handle pyroclastic flows (right). The pictures are annotated real photographs.

observed on pictures of real volcanic ejections, where small vortices of about a meter wide can be distinguished. These solutions are therefore not well adapted to CG applications such as VFX, where visual details, efficient computation, and controllable results are of utmost importance.

Nevertheless, these simulations are based on physical laws expressing the macroscopic interaction between the volcanic column and the ambient air [15, 27], or the effect of the wind [28]. We reuse these laws, which are of great interest for real-time visual simulation. In addition, general knowledge on volcanic column shape and dynamics is typically reported by volcanologists as abacuses and measured curves [2, 9, 23, 34, 35]. These curves depict global phenomena such as the general profile of a plume or the temporal evolution of the ascending velocity. Being generally specified for a specific set of standard conditions, they are not sufficient to generate a full, 3D geometric representation. In this work, we use them as references for validating the physical plausibility of our results.

Note that we developed our solution in collaboration with geoscientists. The fact that we use the same physical laws can make our interactive model relevant in their field, eg. to quickly test various parameters values before launching a more precise simulation. Moreover, in contrast with coarse Eulerian-based simulations which fail to capture interactions with the actual terrain topography, we make use of an accurate terrain model, which can be a plus in predictive applications.

3 OVERVIEW

Our algorithm is based on knowledge in the volcanology of eruptive columns, which we first explain, before describing our model.

3.1 Explosive eruption columns in nature

Volcanic gas and ash particles are released from volcanic vents at high velocity (typically 50 to 200 m/s) as a high density mixture (a few hundred kg/m^3). During an initial *jet phase*, the volcanic mixture is principally propelled from its initial momentum. As the mixture is denser than the atmosphere, it slows down rapidly due to its weight. However, the mixture flows in a turbulent regime, and therefore constantly *entrains* the surrounding air, which gets heated in contact with hot ash particles. Therefore, the fraction of gas increases, which results in a decrease of the mixture density, and thus in an expansion of the column volume. Two possible regimes, presented next, can therefore emerge.

If the rising mixture becomes less dense than the surrounding cooler air, it becomes propelled by buoyancy. The initial jet column then turns into a characteristic volcanic plume mainly driven by buoyancy. This eruption type is called *Plinian regime*. As the vertical decrease of density is slower for the rising parcels than for the surrounding atmosphere (due to the effect of humidity in the troposphere, and then of the heating due to UVs absorption by the ozone layer in the stratosphere), this rise can continue until reaching a maximal altitude characterized by a neutral buoyancy level –i.e. density equality– which can typically happen at a height of tens of kilometers. Near this maximal altitude, the mixture spreads laterally and typically expands along atmospheric winds.

In reverse, if the upward velocity vanishes while the mixture is still denser than the surrounding air, it falls back and generates a pyroclastic flow, also called the *PelÃĺan regime* of the eruption. As the mixture slides and spreads along the terrain slope, the heaviest particles and some ashes settle onto the ground. Therefore, the density of the pyroclastic flow decreases, eventually below the density of the surrounding air. In this case, the buoyancy force allows the mixture to rise again, which leads to the appearance of sub-columns along the spreading region. These sub-columns, however, have a smaller radius and are slower than the one directly above the vent because their initial velocity and turbulence are lower.

Note that a volcano can produce these two ejection regimes and that the type of ejection may even change over time. A famous example is the eruption of Mount Vesuvius, 79 AD, which started as a *Plinian regime* before switching suddenly to *PelÃĺan* leading to the destruction of Pompeii by the pyroclastic flow.

3.2 A layered model for volcanic ejection

The main insight of our model is to decouple the computation of the global dynamic behavior of the mixture ejected by a volcano from the generation of local motion within the resulting, turbulent

flow. Indeed, global dynamics can be efficiently evaluated using a geometrically simplified, yet physically-accurate model. In reverse, a procedural model, carefully coupled with the first one for consistency, is sufficient to generate the necessary amount of animated details at the benefit of low computational costs. These two coupled sub-models form a layered representation of the whole phenomenon, detailed below.

Dynamic simulation layer: The first layer aims at modeling the dynamics and global shape of the ejection column from medium scales (tens of meters) to large scales (several kilometers). This layer is grounded in volcanological studies [23] which tell us that the local parameters in an ejection column are a function of the distance to the column's center-line and the altitude. Therefore, we represent the ejection column, at a large scale, as a generalized cone. As already explained, the turbulent flow entrains and heats the surrounding air, and consequently, the volume of the column increases as it rises. The key idea of the first layer is to simulate this coupled phenomenon at a medium scale by considering a series of radial, cylindrical slices representing a vertical sampling of the whole generalized cone (see Fig. 2-left). These slices are initialized near the volcano vent to the amount of material ejected during a given time interval, characterized by spatially averaged physical quantities (position, velocity, density, temperature). These values, as well as the volume and orientation of the slices, evolve over time, as will be detailed in Sec. 4. The radius and height of the slices are set to a common characteristic size r representing the radius of the largest vortex inside the slice. This size, initialized to the vent's radius r_0, increases with the raise of the column.

Procedural details layer: The coarse dynamic model we just described requires the addition of turbulent details, which we achieve through our second layer, a medium to small scales visual representation of the turbulent flow. In a highly turbulent flow as the eruptive column, multiple vortex rings are intricately mixed and their toroidal structure cannot be clearly distinguished. To represent this billowing motion, we reuse the idea of rotating spheres [5, 12], by embedding the latter in column slices as shown in Fig. 2-middle. This representation, detailed in Sec. 5, efficiently captures animated visual details, up to the scale of a meter.

Pyroclastic flows. can be animated using a simple extension of this layered model (see Fig. 2-right). Unlike the rising plume, these flows fall down along the terrain. We propose to reuse a single intermediate resolution of the second layer's sphere-based representation to compute the propagation of these flows. These spheres, seen as material particles, allow a simple and efficient computation of the interactions with the terrain. To model the possible formation of rising sub-columns where the mixture becomes buoyant again, we turn back to our first layer and emit new dynamic slices covering the areas where the mixture density is low. We then reuse our full column layered model on these new slices, with adapted initial conditions. We provide more details on this extension in Sec. 6.

4 DYNAMICS OF VOLCANIC COLUMNS

We use a Lagrangian simulation with discrete time-steps Δt to compute the dynamic evolution of volcanic eruption columns. As previously described, each simulated element is a cylindrical slice that represents a limited amount of ejected, gas, and ash mixture.

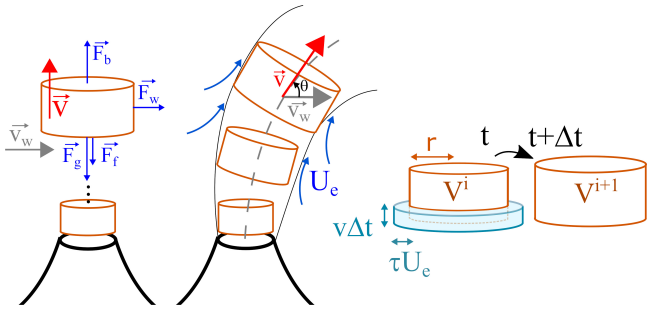

Figure 3: *Left*: **Forces applied to a plume slice.** *Middle*: **Effect of wind on the path and orientation of slices.** *Right*: **Increase of slice volume at each time step, considering the entrained air represented by the blue ring.**

4.1 Evolution of the ejection velocity

A new slice is emitted from the vent every $t_{slice} = r_0/(2\,v_0)$ seconds, depending on the emission speed v_0 and the vent radius r_0. The slice is parameterized using five independent quantities that vary over time: First, its characteristic size r (in m), which represents both the radius and height of the slice (vorticity ring with vortex of radius r) and gives its volume $V = \pi r^3$; Second, the position of its center $\vec{p}$, and in particular its altitude z (in meters); Lastly, the velocity $\vec{v}$ (in m/s), the density ρ (in kg/m^3), and the temperature T (in K) of the slice. In our Lagrangian representation, these three last parameters stand for averaged values of spatial distributions of the modeled quantities over the volume of the slice.

Since the mass $M = \rho V$ of a slice evolves over time due to entrained air, the fundamental equation of dynamics writes as $\mathrm{d}(\mathrm{M}\,\mathrm{v})/\mathrm{dt} = \mathrm{F}$, where $\vec{F}$ is the sum of all forces applied on the slice (detailed in Sec. 4.2). Considering a finite variation of mass ΔM and velocity $\Delta\vec{v}$ during the time interval Δt, we get:

$$\Delta M\,\vec{v} + M\,\Delta\vec{v} = \Delta t\,\vec{F}. \tag{1}$$

Let us call x^i (resp. x^{i+1}, x^{i-1}) a value evaluated at the current (resp. next, previous) time step. We aim to discretize relation (1) with an explicit finite difference scheme expressing the updated velocity $\vec{v}^{i+1}$ with respect to the quantities computed from the current or previous time steps. This expression is not straightforward in the case of volcanic column dynamics, as the change of mass depends on velocity. To avoid an implicit, non-linear relation on $\vec{v}^{i+1}$ that appears in both $\Delta\vec{v}$ and ΔM, we inspire from symplectic Euler schemes and evaluate ΔM at the previous time step:

$$(M^i - M^{i-1})\,\vec{v}^i + M^i(\vec{v}^{i+1} - \vec{v}^i) = \Delta t\,\vec{F}^i\,, \tag{2}$$

which finally leads to the explicit relation:

$$\vec{v}^{i+1} = \frac{M^{i-1}}{M^i}\,\vec{v}^i + \Delta t\,\frac{\vec{F}^i}{M^i}\,. \tag{3}$$

4.2 Modeling the applied forces

The force $\vec{F}$ applied to each slice is split into four contributing components (see Fig.3-left), namely the weight $\vec{F}_g$, buoyancy $\vec{F}_b$, friction $\vec{F}_f$, and wind force $\vec{F}_w$. The slice weight is computed as $\vec{F}_g = M\,\vec{g}$, where $\vec{g}$ is the gravity constant. Buoyancy is set to:

$$\vec{F}_b = -\rho_a(z)\,V\,\vec{g}\,, \tag{4}$$

where ρ_a is the density of the atmosphere (outside of the volcanic column) at the slice altitude z. The variation of velocity between the column and the surrounding air induces a shear stress $\tau = \rho_a C_d v^2$ in turbulent flows, where $v = \|\vec{v}\|$ and C_d is a dimensionless drag coefficient. This stress induces a friction force acting on the lateral slice boundaries (in contact with the air), of area $S = 2\pi r^2$:

$$\vec{F}_f = -\frac{1}{2}\rho_a\,C_d\,S\,v^2\;\;\vec{v}/v\,. \tag{5}$$

Note that this force term is necessary for our bounded slice model, contrary to previous studies that relied on approximate radial velocity profiles tending to zero as r goes to infinity [15]. Finally, we model the force exerted by a horizontal wind of velocity $\vec{v}_w$, as:

$$\vec{F}_w = \lambda\,S_{\text{eff}}\,\|\vec{v}_w - \vec{v}_{|xy}\|\,(\vec{v}_w - \vec{v}_{|xy})\;\;, \tag{6}$$

where $\vec{v}_{|xy}$ is the velocity component of the slice in the horizontal plane, $S_{\text{eff}} = 2r^2$ is the effective cross-section of the slice where the wind acts, and λ is a constant coefficient.

4.3 Evolution of a slice's size and density

The applied forces listed above depend on the size of the slice, i.e. its radius r from which surface and volume are computed, as well as on its mass. These quantities are evolving over time due to the entrainment of the surrounding air during the ascending phase. Let us describe our model for this evolution.

We rely on the notion of *entrainment velocity* [28] U_e, used in volcanic models to express, at the macroscopic scale, the averaged velocity at which the surrounding ambient air is incorporated and mixed within the turbulent plume. In the absence of wind, U_e is assumed to be proportional to the speed of the plume $U_e = k_s|v|$, where k_s is a *coefficient of entrainment*. In the case of wind of magnitude v_w, the relative contributions of the wind on the vertical and horizontal planes are modeled in volcanology as different and additive, leading to:

$$U_e = k_s\,|v - v_w\cos(\theta)| + k_w\,|v_w\sin(\theta)|\,, \tag{7}$$

where θ is the angle between $\vec{v}$ and $\vec{v_w}$ (see Fig. 3-middle).

This entrainment velocity is used at each time step to compute the newly incorporated volume of surrounding air within the slice. To this end, we consider such volume to be geometrically defined as a cylindrical ring with radius spanning the interval $[r, r+\tau U_e]$, and of height $v\,\Delta t$, giving an additional volume $\pi\,((\tau\,U_e + r)^2 - r^2)\,v\,\Delta t$ as illustrated in Fig. 3-right.

The mix between the newly incorporated air and the current plume impacts the physical parameters of the slice, which are updated as follows: We first compute the new averaged temperature T^{i+1} assuming that the global heat capacity of the new mixture remains constant ($M_a^i = \rho_a(z)\,U_e^i\,v^i\,\Delta t^2$ being the mass of the entrained air, and $T_a(z)$ a standard normalized temperature model of the atmosphere at altitude z):

$$T^{i+1} = \frac{M_a^i T_a(z) + M^i T^i}{M_a^i + M^i}\,, \tag{8}$$

This change of temperature results in a change of slice volume, from V^i to $V^{i\prime}$ for the slice and V_a to $V_a{}'$ for the atmosphere annulus, and obtained from the perfect gas equation: $V^{i\prime} = V^i\;T^{i+1}/T^i$, and $V_a' = V_a\;T^{i+1}/T_a(z)$. The new volume of the slice is the sum of these two new volumes, and the new radius and height, set to the same value r^{i+1}, are computed from the equation of a cylinder's volume as $r^{i+1} = \sqrt[3]{(V^{i\prime} + V_a{}')/\pi}$. In addition to the entrainment of air, the mixture of the slice also slowly sediments, leading to the loss of the heaviest particles that fall down and leave the slice. We model this phenomenon by assuming a constant decrease of mass σ_{col} over time. The updated total mass of the slice is, therefore:

$$M^{i+1} = M_a^{i+1} + M^i - \sigma_{col}\Delta t\,. \tag{9}$$

and, the new slice density can be computed as $\rho^{i+1} = \frac{M^{i+1}}{V^{i+1}}$.

Independently from these parameters, the slices are always oriented orthogonally to their trajectory during their ascending phase, in accordance with the assumption that each slice contains a large vortex ring constrained to translate orthogonally to the central axis.

5 PROCEDURAL DETAILS AND UMBRELLA

5.1 Multi-resolution, rotating spheres

As explained in Sec. 3.2, billowing volcanic flows take the visual appearance of rotating spheres at multiple scales, of expanding sizes during ascent. In this section, we detail our second layer, which models this rich visual appearance, using procedural spheres guided by simulated slice dynamics (see Fig. 2-middle).

At the largest scale s_1, the rotating spheres have a radius similar to the characteristic length r of a slice and exhibit a convective motion relative to the main averaged ascending movement. More precisely, the convection drives a toroidal motion (upward velocities close to the central axis of the column, downward at the boundaries), which can be represented by vortex rings [3]. To imitate the toroidal motion, we associate to each slice a vortex ring, defined by an inner circle with same position and orientation as the slice, and with radius $r/2$. We then uniformly sample n overlapping spheres of radius $r/2$ so that their center lies on the inner circle, and perturb the position and scaling of the spheres by a small factor to achieve natural variations. The velocity of the spheres is set to the slice velocity $\vec{v}$, while the angular velocity $\vec{\Omega_s}$ is given as a boundary condition enforcing the velocity at the exterior of the column to be equal to the air velocity: $\vec{\Omega_s} = v_s/r_s\vec{t_s}$, where $\vec{t_s}$ is the unit vector tangent to the inner circle and oriented clockwise.

The surface of the spheres in s_1 is sampled by a series of recursively defined, smaller spheres, in order to model the cascading vortices of the turbulent flow. Based on observation, we typically consider two more layers of spheres s_2 and s_3, of radius decreasing by a factor five from a sphere to its parent. In our experiments, this leads to a size of about a meter for the smallest visible details, generated by the smallest s_3 spheres located near the volcano vent. Each child sphere is initialized at a random position on its parent

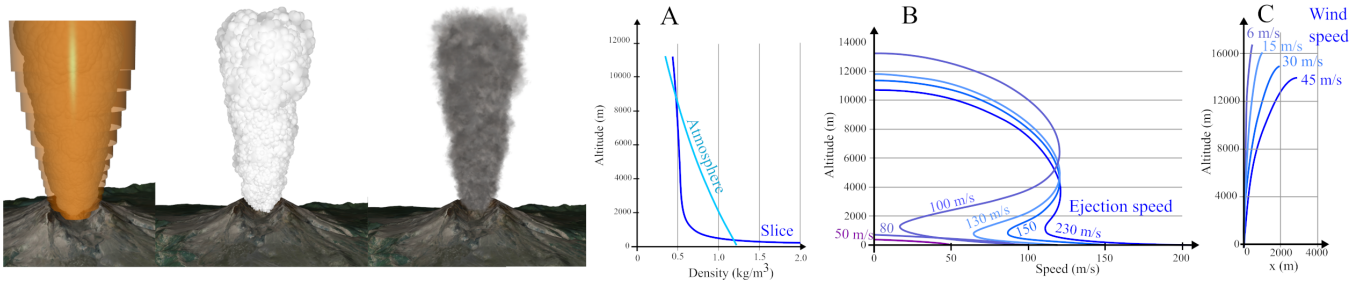

Figure 4: Left: Real-time previsualization of the column dynamics showing respectively the slices; the first and second scale spheres; rotating billboard. Right: Validation of the evolution of the simulation parameters. A: Evolution of the density of the column with respect to the altitude, compared to the density of the standard atmosphere (for a given ejection speed and no wind). B: Evolution of the altitude and vertical speed of a slice for different ejection speeds. C: Trajectory of a slice displayed in a 2D graph when a constant horizontal wind is applied. Stronger wind velocity leads to a lower maximal altitude.

sphere and is rigidly attached to the motion of the latter. This allows to better perceive the general rotational motion at scale s_1.

5.2 Procedural umbrella over the plume

When the altitude $z_{neutral}$ of equilibrium density is reached, the pressure from the underlying rising column, which continuously brings new material, leads to a horizontal spread of the flow. The latter then takes a characteristic *umbrella* shape.

Our model for animating this umbrella is twofold: First, at the end of the ascending phase, the column trajectory slightly *over-shots* beyond the neutral buoyancy altitude $z_{neutral}$ due to inertia. This phenomenon, which can be observed in real eruption footage, is already captured by the dynamic simulation used for slices. Second, once this *overshot* maximal altitude is reached, we *detach* the large scale spheres from their associated slice, and procedurally adapt their individual trajectories to animate a smooth transition from ascending motion to horizontal spreading.

To this end, we compute radial motion as to ensure volume conservation: We consider that a slice reaching $z_{neutral}$ with a vertical velocity v then expands radially with the same velocity. During an infinitesimal time ∂t, the volume of this slice (initially defined by $V = \pi r^3$) then increases by $\partial V = \pi r^2 v\, \partial t$. To accommodate for this expansion, all material at distance d from the central axis of the column needs to increase by $\partial V = \pi r\, dv\, \partial t$, leading to a new velocity $v_{umbrella}(d) = v\, r/d$ for the spheres, d being the radial distance to the center of the rising column. Lastly, we generate a smooth asymptotical descending motion for each sphere toward their final altitude $z_{neutral}$, using a procedural decreasing function shaped as $1/d$.

6 MODELING PYROCLASTIC FLOWS

Depending on the initial density and ejection speed, the volcanic column may not reach the critical amount of buoyancy to compensate for its weight. In this case, the ash mixture falls down shortly after its ejection and leads to a pyroclastic flow.

Our model switches to pyroclastic behaviour during simulation (after the evaluation of Eq. (3)), if a slice's velocity becomes negative before reaching the neutral buoyancy altitude. In this case, we trigger specific pyroclastic effects, which requires a few modifications of our layered model. Two phenomena need to be modeled. First, the propagation of the descending ash and gas mixture down the terrain slope, and second, the possible formation of ascending sub-columns, due to the loss of density of the mixture related to ash sedimentation (see Fig. 2-right).

We rely on the four forces already described in Sec. 4.2 (weight, buoyancy, friction, and wind force) to simulate the dynamics of the pyroclastic flow. However, since the pyroclastic flow descends the slope of an arbitrary terrain, its complex geometry cannot be captured by our cylindrical slice model. Therefore, we replace the falling slice geometry with a set of falling spheres initialized to uniformly fill the slice's volume. In practice, we use the scale s_2 of our sphere layers, to provide enough degrees of freedom.

Each sphere is assumed to be an independent particle simulated under the actions of weight, buoyancy, friction, and wind forces. The expression of these forces is adapted to the geometry of the spheres, whose volume is supposed to remain unchanged, despite sedimentation, during flow propagation. The interaction with the terrain, modeled using collision with a height field surface, allows to efficiently model the spread of the flow along the slope. During this spread, the mixture sediments the heaviest particles, which we model as a constant mass decrease over time, by a factor σ_{pyr}.

As the mixture loses weight and density, the simulated spheres may become buoyant and elevate again in the air. We use a clustering method to identify groups of near-by buoyant spheres with relative distance smaller than r_{pyr} that will trigger the creation of a rising column using the method in Sec. 4, but with different initial conditions. The clustered spheres are replaced by new rising slices starting from their centroid, with a characteristic size r_{pyr}. To preserve mass and momentum, the initial density and velocity of the slices are set to the average of those of the clustered spheres, which are then removed. Once created, the new columns follow the same simulated model as the primary column and can be pushed by the wind. Note that the pyroclastic flow progressively brings new buoyant spheres, which are converted to slices added to the volume of the rising sub-columns, eventually over a large area. As opposed to vent ejection which (a continuous and localized flow source), each slice creation in a pyroclastic flow happens at a given time, but the process repeats at various ground positions.

7 VISUALIZATION AND RESULTS

7.1 Real-time animation and rendering

We implemented a real-time graphics prototype as a single thread C++ code with OpenGL display and run it on a consumer laptop (Intel Core i7 2.6GHz CPU, NVidia Quadro P3200 GPU, 16GB RAM).

Visualization: As illustrated in Fig. 4-left, our prototype allows to visualize the slices and spheres, as well as to convey a fuzzy appearance using billboards. In the latter, smoke-like texture is mapped on quadrangles facing the camera and following the center and dimension of the spheres, while their angular speed in the camera plane is expressed as the projection of the 3D angular velocity of the slice onto the forward direction of the camera.

Performance: Although not optimized, our implementation runs at more than 60 fps for all our examples. We used up to 80 slices and visualized the two first sphere scales (see accompanying video). If needed, higher levels of details could be displayed, but may need acceleration using graphical tessellation or instancing.

Model parameters: Table 1 provides the default values for our parameters. r_0, ρ_0, and T_0 correspond to standard volcanic measures. Our empirical, drag coefficient C_d matches the expected order of magnitude for the standard aerodynamics model. We used values from [34] for (k_s, k_v). The other coefficients were tuned empirically.

Simulation time step	Initial density	Vent radius
Δt 0.002s	ρ_0 200kg/m^3	r_0 100m
Initial temperature	Drag coeff.	Wind force coeff.
T_0 1273K	C_d 0.04	λ 600
Entrainment coeff.	Air entrainment coeff.	# spheres/slice
(k_s, k_v) (0.09,0.9)	τ 5s	n 6
Column sedim. coeff.	Pyroclastic sedim. coeff.	Secondary col. size
σ_{col} 5×10^{-8}	σ_{pyr} 5×10^{-6}	r_{pyr} r_{s_2}

International Standard Atmosphere model

$\rho_a(z) = 353 \frac{(1-2.3\times10^{-5}z)^{5.3}}{288-6.5\times10^{-3}z}$, $T_a(z) = 288 - 6.5 \times 10^{-3}\, z$

Table 1: Parameters used in our simulation.

Our model allows the user to dynamically tune them at run time, as illustrated in the companion video. For instance, the emission velocity and density, the wind direction and orientation at a different angle, or even the vent radius, can be easily changed. Such interactive control on simulation parameters, coupled with real-time computations, is essential to explore various behaviors for educational purposes, or in virtual museums. It can also be used for quickly testing new hypotheses in volcanology applications before running a costlier simulation on a restricted domain.

7.2 Validation of Column Dynamics

We analyzed the numerical results of our column dynamic model and plot in Fig. 4 curves that can be found as references in volcanology literature. Fig. 4-A shows the evolution of the density of a slice ejected at an average velocity of 150m/s with respect to its altitude. As expected [14, 35], the density decreases quickly at low altitude, and cross a first time the atmospheric density to become lighter than the surrounding air. The slice then becomes propelled by buoyancy until reaching 9km where the slice density and the atmosphere reach again an equal density. The slice slightly exceeds this altitude due to inertia and ends up reaching a final equilibrium. Fig. 4-B represents the evolution of the altitude of a rising slice with respect to its vertical speed. The multiple curves displayed correspond to different initial velocities at the vent. These curves are consistent with the one reported by Carey et al. [2] (Fig.32.3) with respect to their general shape and behavior relative to the emission velocity. In the case of an emission velocity below 80 m/s, a quick decrease of the vertical speed is obtained as the mixture doesn't get buoyant and falls back as pyroclastic flows. For higher initial speed, after the initial slow down, the column gains temporary speed due to the buoyancy propelling at low altitude, which leads to the noticeable inflection of the curves also reported in [2]. Finally, the velocity slowly decreases near its maximal altitude. Fig. 4-C reports the trajectory appearance of the central line of the column when winds with various magnitudes are applied. For these measurements, we consider wind profiles that linearly increase from a zero magnitude on the ground to the maximal specified value at 12 km height. The curves we obtain can be compared to the one reported in Woodhouse et al. [34] (Figure 2) relative to the Eyjafjallajökull eruption in 2010 using the same wind profiles, with agreement on the characteristic bent trajectory, as well as the fact that higher wind velocity leads to lower maximal altitude.

7.3 Off-line Rendering

Once the user is satisfied with the real-time simulation, the spheres data can be exported to an external volume-based renderer. We use Houdini [21], which is set up to convert a set of spheres to an implicit surface. We create a 500^3 voxel grid and store the distance to the surface (using a Signed Distance Function, or SDF) in a narrow band of 6 voxels around it. In this band, we consider a smooth *visual-density* used by the Houdini's built-in volumetric renderer, while taking into account the two following features: First the per-sphere material density ρ that decreases with elevation, capturing the smoother and less dense appearance for the ejection flow at high altitudes. Second, we ensure a smooth rendering of the flow boundary by rescaling and clamping the SDF so that the resulting *visual-density* is 1 inside the plume and smoothly transitions toward 0 at the exterior. We then multiply this *visual-density* with a lower-dimension one, computed on a volume of (100^3) where we sub-sampled the per-sphere material density. We finally add small details below the scale of the smallest spheres using a cellular Worley noise. In practice, our off-line rendered scenes use 5 to 20 million individual spheres to generate the required density.

7.4 Final results

We simulated and rendered animations for several scenarios. Fig. 5-top shows the evolution of a rising plume with an ejection speed of 150 m/s and no wind. We can see the gas and ashes mixture spread symmetrically from the central plume when reaching the neutral buoyancy altitude, in agreement with real photography shown in the right part. In comparison, Fig. 1-middle, Fig. 5-bottom and the accompanying video show the result of a similar ejection speed, but in the presence of left-to-right wind. The umbrella spreads slightly

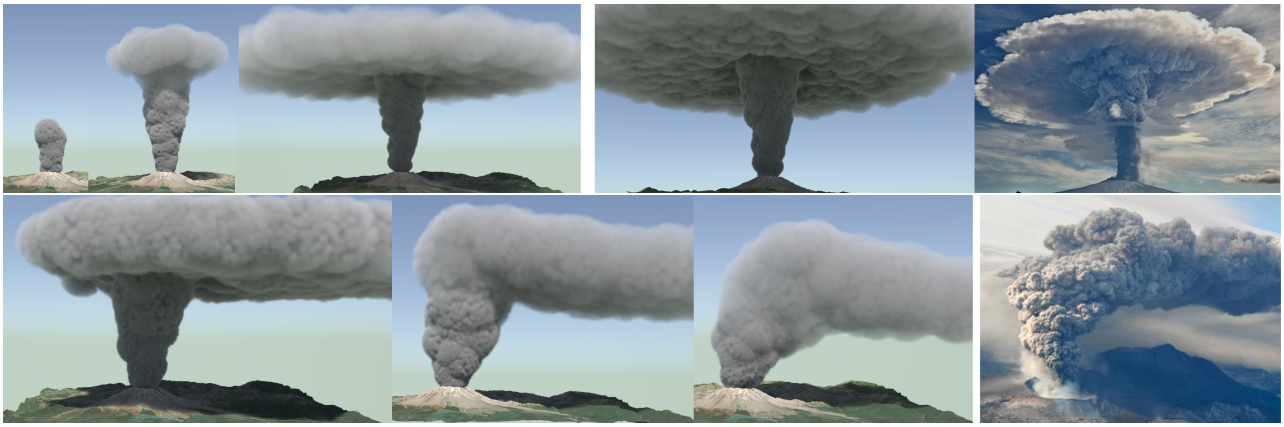

Figure 5: Top: Evolution of a rising plume through time and its spreading umbrella shape in the atmosphere (off-line rendering) compared to a real photograph at the right. Bottom: Effect of an increasing wind of 15, 45, and 105 m/s on the column profile (off-line rendering) compared to a real photograph.

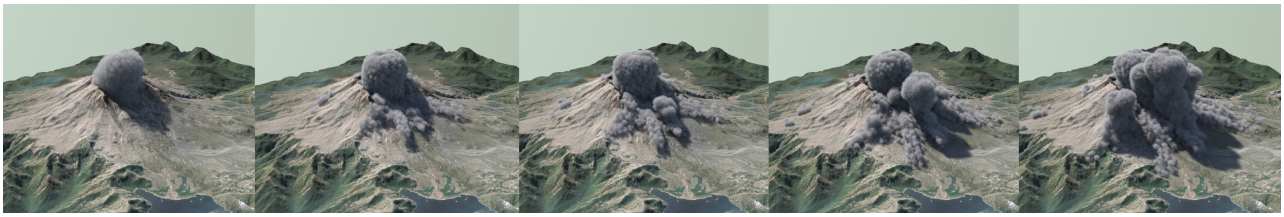

Figure 6: Pyroclastic flows animation: from left to right, the column begins to fall down; the pyroclastic flows go down the slopes of the volcano; secondary columns appear above the flows; secondary columns rise (off-line rendering).

non-symmetrically under a weak wind, while its propagation becomes almost unidirectional under stronger winds. Fig. 6 and the companion video show a time-lapse of a pyroclastic flows animation. In this case, the ejection speed of the column is about 70 m/s, which is too low to enable the ejected column to become buoyant. The mixture then falls back along the slopes of the volcano (three first pictures). In the last picture, sub-columns start to raise from spheres clusters that lost enough weight to become less dense than the air.

8 CONCLUSION AND FUTURE WORK

We presented a layered model for the real-time animation of volcano ejection. The first layer of our model is a lightweight Lagrangian simulation based on a discretization of the rising column into slices. This combination of cylindrical geometry and dynamic simulation allows handling physical phenomena that were never modeled in CG but are at the core of ejection dynamics such as air entrainment, drastic density variations, and volume expansion over large distances. Our dynamic model also triggers the automatic switch between jet and buoyancy propelling. The scale of the slice, which expands over time, represents the scale of the largest vortices at a given height, and can therefore be easily visually enriched while preserving real-time performances, using a second layer. The latter is composed of a multi-scale set of spheres representing the billowing aspect of the turbulent flow. We also reused these two layers to represent pyroclastic flows, where a simple sphere model is used to compute the spread of the ejection along the terrain slope, while sub-columns are generated using the previous Lagrangian simulation where and when the mixture becomes buoyant again. While remaining an approximation, our model is consistent with respect to real volcano dynamics, as shown by our comparisons of velocity and density values over time with reference data from volcanology literature. In addition, it brings plausible visual results, which can be pre-visualized in real-time to ease parameter tuning.

Our layered model suffers inherent limitations since each element is designed to match some expected behavior. Such lightweight model is a trade-off between realism, speed, and control, and is restricted to the actual phenomena it was designed for, here ejections from explosive volcanic eruptions. This limits its usability in other types of eruptions, *e.g.,* effusive ones where lava flows are to be combined with smoke.

Our current prototype could however be easily improved: The Kolmogorov cascade of details modeled by the spheres could be enhanced by adding sub-motions at the lower scale, and by using different sizes for the smaller spheres. Faster volumetric rendering and adapted shaders available in standard game engines could also be used to improve the rendering of the interactive simulator.

As future work, we would like to couple our volcanic eruption model with lightweight atmospheric simulation, to visualize the condensation phenomena associated with the fast rising motion

of entrained, humid air. Adding the visualization of ash rain and lightning would also improve the realism of our results. Another avenue for research, made easier by our layered model, would be its inverse simulation, enabling to enrich artistic control by pre-setting or even sketching characteristic features of the ejection such as maximal elevation, column shape, or pyroclastic spread, with some automatic tuning of simulation parameters. Finally modeling and simulating realistic lava flows in real-time would also be of interest for a full volcanic eruption model.

REFERENCES

[1] Alexis Angelidis, Fabrice Neyret, Karan Singh, and Derek Nowrouzezahrai. 2006. A Controllable, Fast and Stable Basis for Vortex Based Smoke Simulation. *SCA* (2006), 25âĂŞ32.

[2] Steven Carey and Marcus Bursik. 2015. *Encyclopedia of Volcanoes - Volcanic Plumes.* University of Chicago Press, Chapter 32, 571–585.

[3] G.-H. Cottet and P. D. Koumoutsakos. 2000. *Vortex Methods: Theory and Practice.* Cambridge University Press.

[4] F. Dobran and J. I. Ramos. 2006. Global Volcanic Simulation: Physical Modeling, Numerics, and Computer Implementation. *Developments in Volcanology* 8 (2006), 311–372.

[5] PDI Dreamworks. 2001. Chapter 'Flames and Dragon Fireballs' in 'Shrek: The Story Behind the Screen'. *ACM SIGGRAPH Course Notes* (2001).

[6] Ronald Fedkiw, Jos Stam, and Henrik Wann Jensen. 2001. Visual Simulation of Smoke. *SIGGRAPH* (2001), 15–22.

[7] Jonathan Gagnon, Julian E. Guzman, Valentin Vervondel, FranÃğois Dagenais, David Mould, and Eric Paquette. 2019. Distribution Update of Deformable Patches for Texture Synthesis on the Free Surface of Fluids. *CGF, Proc. Pacific Graphics* 38 (2019).

[8] Torsten Hadrich, Milosz Makowski, Wojtek Palubicki, Daniel T. Banuti, Soren Pirk, and Dominik L. Michels. 2020. Stormscapes: Simulating Cloud Dynamics in the Now. *ACM TOG, Proc. SIGGRAPH*, Article 175 (2020), 16 pages.

[9] Claude Jaupart. 1996. Physical models of volcanic eruptions. *Chemical Geology* 128 (1996), 217–227.

[10] Chenfanfu Jiang, Craig Schroeder, Andrew Selle, Joseph Teran, and Alexey Stomakhin. 2015. The Affine Particle-In-Cell Method. *ACM TOG, Proc. SIGGRAPH*, Article 51 (2015), 10 pages.

[11] James T. Kajiya and Brian P Von Herzen. 1984. Ray Tracing Volume Densities. *SIGGRAPH Computer Graphics* (1984).

[12] Alan Kapler. 2003. Avalanche! Snowy FX for XXX. In *ACM SIGGRAPH 2003 Sketches & Applications.* ACM.

[13] MFiX. 2021. Multiphase Flow with Interface Exchange. https://mfix.netl.doe.gov/

[14] Ryoichi Mizuno, Yoshinori Dobashi, and Tomoyuki Nishita. 2002. Volcanic smoke animation using CML. *Proc. Int. Computer Symposium* (2002).

[15] B. R. Morton, G. I. Taylor, and J. S. Turner. 1956. Turbulent gravitational convection from maintained and instantaneous sources. *Proc. R. Soc. London* 234 (1956), 1âĂŞ–23.

[16] Rahul Narain, Vivek Kwatra, Huai-Ping Lee, Theodore Kim, Mark Carlson, and Ming Lin. 2007. Feature-Guided Dynamic Texture Synthesis on Continuous Flows. *Rendering Techniques, Proc. Symp. on Rendering* (2007), 361–370.

[17] Fabrice Neyret. 1997. Qualitative Simulation of Cloud Formation and Evolution. In *EG Work. on Comp. Anim. and Simulation.*

[18] Sanjit Patel, Anson Chu, Jonathan Cohen, and Frederic Pighin. 2005. Fluid Simulation Via Disjoint Translating Grids. *ACM SIGGRAPH Sketches* (2005), 139âĂŞ–es.

[19] H. Schechter and R. Bridson. 2008. Evolving Sub-Grid Turbulence for Smoke Animation. *Symp. on Computer Animation* (2008), 1âĂŞ7.

[20] Maurya Shah, Jonathan M. Cohen, Sanjit Patel Penne Lee, and FrÃĪdÃĪric Pighin. 2004. Extended Galilean Invariance for Adaptive Fluid Simulation. *Symp. on Computer Animation* (2004), 213âĂŞ–221.

[21] SideFX. 2021. Houdini. https://www.sidefx.com

[22] Dan Sotra, Pierre-Olivier Agliati, Marie-Paule Cani, Fabrice Neyret, and Jean-Dominique Gascuel. 1999. Animating Lava Flows. *Graphics Interface* (1999), 203–2010.

[23] R. Sparks. 1986. The dimensions and dynamics of volcanic eruption columns. *Bulletin of Volcanology* 48 (1986), 3–15.

[24] Jos Stam. 1999. Stable Fluids. *SIGGRAPH* (1999), 121–128.

[25] Alexey Stomakhin, Craig Schroeder, Chenfanfu Jiang, Lawrence Chai, Joseph Teran, and Andrew Selle. 2014. Augmented MPM for phase-change and varied materials. *ACM TOG, Proc. SIGGRAPH* 33, 4, Article 138 (2014), 11 pages.

[26] Y. J. Suzuki, A. Costa, M. Cerminara, T. Esposti Ongaro, M. Herzog, A. R. Van Eaton, and L. C. Denby. 2016. Inter-comparison of three-dimensional models of volcanic plumes. *Journal of Volcanology and Geothermal Research* 326 (2016), 26–42.

[27] Y. J. Suzuki and T. Koyaguchi. 2010. Numerical determination of the efficiency of entrainment in volcanic eruption columns. *Geophysical Research Letters* 37, 5 (2010), L05302–.

[28] Y. J. Suzuki and T. Koyaguchi. 2015. Effects of wind on entrainment efficiency of wind on entrainment efficiency in volcanic plumes. *Journal of Geophysical Research: Solid Earth* 120 (2015), 6122–6140.

[29] C. Textor, H.-F. Graf, A. Longo, A. Neri, T. Esposti Ongaro, P. Papale, C. Timmreck, and G. G.J. Ernst. 2005. Numerical simulation of explosive volcanic eruptions from the conduit flow to global atmospheric scales. *Annals of Geophysics* 48 (2005).

[30] Nils Thuerey, Theodore Kim, and Tobias Pfaff. 2013. Turbulent Fluids. *ACM SIGGRAPH Course Notes* (2013).

[31] Ulysse Vimont, James Gain, Maud Lastic, Guillaume Cordonner, Babatunde Abiodun, and Marie-Paule Cani. 2020. Interactive Meso-scale Simulation of Skyscapes. *CGF, Proc. Eurographics* 39, 2 (2020).

[32] Steffen Weißmann and Ulrich Pinkall. 2010. Filament-Based Smoke with Vortex Shedding and Variational Reconnection. *ACM Transaction on Graphics* (2010).

[33] Maximilian Werhahn, You Xie, Mengyu Chu, and Nils Thuerey. 2019. A Multi-Pass GAN for Fluid Flow Super-Resolution. *Symp. on Computer Animation*, Article 10 (2019), 21 pages.

[34] M. J. Woodhouse, A. J. Hogg, J. C. Philips, and R. S. Sparks. 2013. Interaction between volcanic plumes and wind during the 2010 Eyjafjallajökull eruption, Iceland. *J. Geophysical Research: Solid Earth* 118 (2013), 92–109.

[35] A. W. Woods. 1988. The fluid dynamics and thermodynamics of eruption columns. *Bulletin of Volcanology* 50, 3 (1988), 169–193.

[36] Shenfan Zhang, Fanlong Kong, Chen Li, Changbo Wang, and Hong Qin. 2017. Hybrid modeling of multiphysical processes for particle-based volcano animation. *Computer Animation & Virtual Worlds* 28 (2017).